[redacted]

NASA TECHNICAL MEMORANDUM

NASA TM SX-3205

FOR

U.S. AIR FORCE

NASA TM SX-3205

ANALYSIS OF THE FLIGHT MOTIONS OF A SMALL DEPLOYABLE GLIDER CONFIGURATION (U)

COORD NO. AF-AM-419

Paul L. Coe, Jr.

Langley Research Center
Hampton, Va. 23665

UNCLASSIFIED

NATIONAL AERONAUTICS AND SPACE ADMINISTRATION • WASHINGTON, D. C. • MARCH 1975

[redacted]

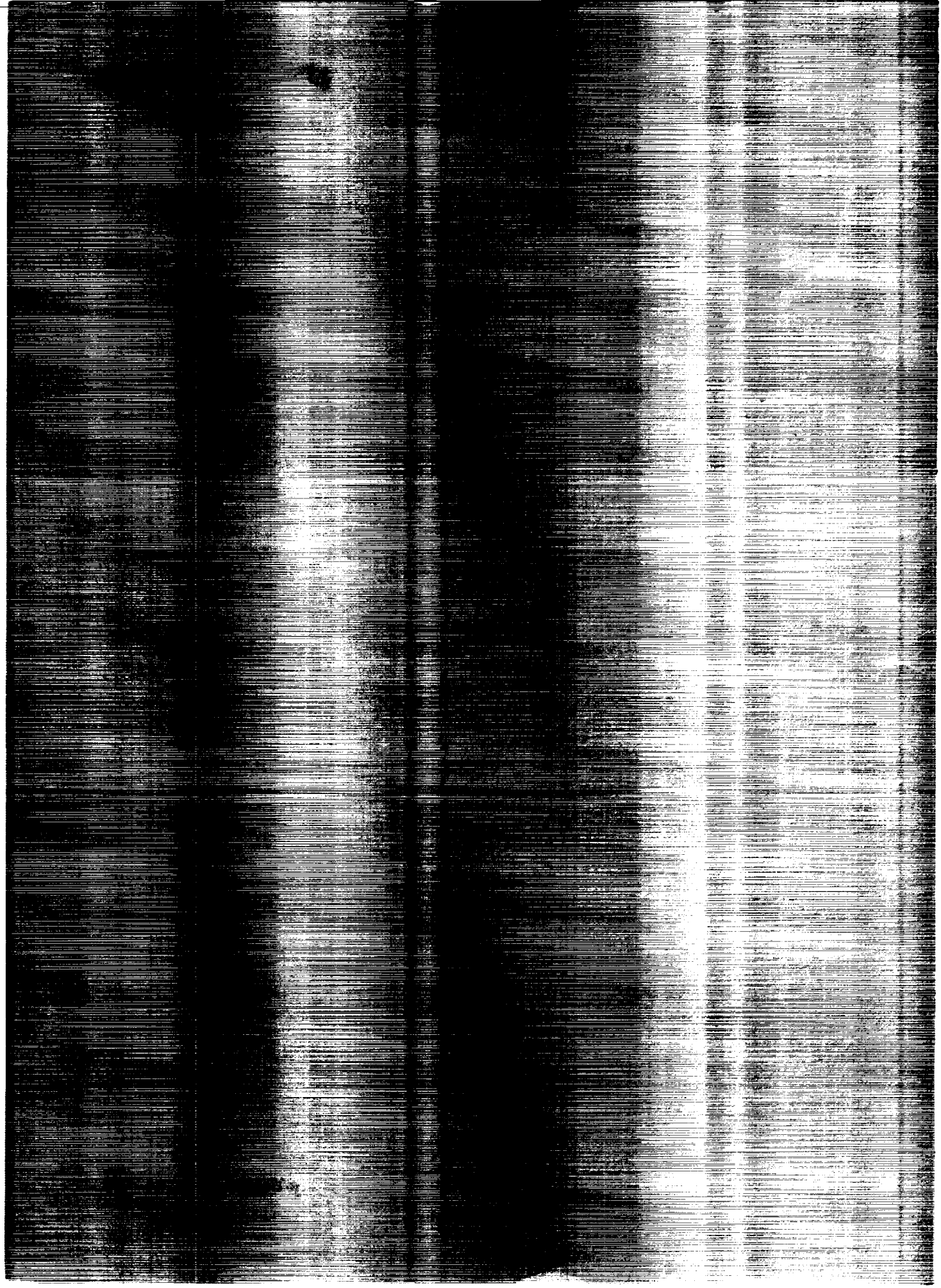

[redacted]

1. Report No.	2. Government Accession No.	3. Recipient's Catalog No.
NASA TM SX-3205		

4. Title and Subtitle	5. Report Date
ANALYSIS OF THE FLIGHT MOTIONS OF A SMALL DEPLOYABLE GLIDER CONFIGURATION – COORD NO. AF-AM-419 (U)	March 1975
	6. Performing Organization Code
7. Author(s)	8. Performing Organization Report No.
Paul L. Coe, Jr.	L-10031
	10. Work Unit No.
9. Performing Organization Name and Address	505-06-81-01
NASA Langley Research Center Hampton, Va. 23665	11. Contract or Grant No.
	13. Type of Report and Period Covered
12. Sponsoring Agency Name and Address	Technical Memorandum
National Aeronautics and Space Administration Washington, D.C. 20546	14. Sponsoring Agency Code

15. Supplementary Notes

Prepared for the U.S. Air Force.

16. Abstract

An investigation was conducted at the request of the U.S. Air Force Avionics Laboratory to analyze the flight characteristics of a small uncontrolled glider with folding wings. The study consisted of wind-tunnel tests of an actual glider and a theoretical analysis of the performance, stability, and trimmability of the configuration.

17. Key Words (Suggested by Author(s))	18. Distribution Statement
Gliders Stability Effect of relative density	The distribution of this document should be restricted to those recipients endorsed by the organization for which it was prepared. New Subject Category 08

19. Security Classif. (of this report)	20. Security Classif. (of this page)	21. No. of Pages	22. Price
Confidential	Unclassified	28	

"NATIONAL SECURITY INFORMATION"

Unauthorized Disclosure Subject to Criminal Sanctions.

CONFIDENTIAL CLASSIFIED
BY AFSC/DOSR dated May 16, 1974
SUBJECT TO GENERAL DECLASSIFICATION SCHEDULE OF EXECUTIVE ORDER 11652 AUTOMATICALLY DOWNGRADED AT TWO YEAR INTERVALS AND DECLASSIFIED ON DEC 31 1976

[redacted]

[redacted]

[redacted]

[redacted]

ANALYSIS OF THE FLIGHT MOTIONS OF A SMALL DEPLOYABLE GLIDER CONFIGURATION (U)

COORD NO. AF-AM-419

Paul L. Coe, Jr.
Langley Research Center

SUMMARY

An investigation was conducted at the request of the U.S. Air Force Avionics Laboratory to determine the cause of a series of unsuccessful test flights of a small uncontrolled glider with folding wings. Initially, contractor tests conducted in a swimming pool indicated that the glider exhibited satisfactory glide capability, trim characteristics, and dynamic stability characteristics. The pool tests were followed by a number of unsuccessful flight tests in air during which the model generally exhibited tight spirals or continuous 360° rolling motions which resulted in an essentially ballistic trajectory.

The present study consisted of wind-tunnel tests of an actual glider and a theoretical analysis of the performance, stability, and trimmability of the configuration. The analysis also defined the factors which probably caused the vastly different motions exhibited by the configuration in air and in water.

The results of the study showed that the proximity of the trim condition to the onset of wing stall, the inherent lateral-directional instability of the configuration, and the existence of large out-of-trim rolling moments created by wing asymmetries were all possible causes for the series of unsuccessful test flights.

INTRODUCTION

An investigation was conducted at the request of the U.S. Air Force Avionics Laboratory to determine the cause of a series of unsuccessful test flights of a small uncontrolled glider with folding wings. In operational use, it was intended that a large number of the gliders, containing electronic countermeasure (ECM) equipment, would be simultaneously deployed from aircraft during tactical missions. Initially, contractor tests were conducted by launching the vehicle under water in a swimming pool in order to determine the performance, and stability of the glider motions. The results of these pool tests indicated that the glider exhibited satisfactory glide capability, trim characteristics, and dynamic stability characteristics. The pool tests were followed by a number

[redacted]

of unsuccessful flight tests in air involving drop tests from a general-aviation airplane at an altitude of 609.6 m (2000 ft). After the launch, the model generally exhibited tight spirals or continuous 360° rolling motions which resulted in an essentially ballistic trajectory. In some instances, however, a few of the gliders appeared to recover from the launch and obtain a momentary wings-level glide that was followed immediately by a sudden wing drop and 360° rolls along a ballistic trajectory. In addition, several flight tests were made with a model with a smaller vertical tail. In these tests the model generally exhibited the same rolling motions; however, a few of the models were seen to exhibit a severe Dutch roll oscillation. As a result of the rapid rolling motions, the various gliders tested exhibited essentially no glide capability, and the configuration was obviously unsuitable for the intended operational mission.

The present study, conducted at the NASA Langley Research Center, consisted of wind-tunnel tests of an actual glider and a theoretical analysis of the performance, stability, and trimmability of the configuration. The analysis also defined the factors which probably caused the vastly different motions exhibited by the gliders in air and in water.

SYMBOLS

All aerodynamic data with the exception of lift and drag are presented with respect to the body system of axes. Moment data are presented with respect to a center-of-gravity position of 25 percent of the wing mean aerodynamic chord. Dimensional values are presented in the International System of Units (SI) with equivalent values given parenthetically in the U.S. Customary Units.

b	wing span, m (ft)
C_D	drag coefficient, $F_D/q_\infty S$
C_L	lift coefficient, $F_L/q_\infty S$
C_l	rolling-moment coefficient, $M_X/q_\infty Sb$
$C_{l,0}$	rolling-moment coefficient at $\beta = 0^\circ$
C_m	pitching-moment coefficient, $M_Y/q_\infty S\bar{c}$
C_n	yawing-moment coefficient, $M_Z/q_\infty Sb$
C_X	longitudinal-force coefficient, $F_X/q_\infty S$

[redacted]

C_Y	side-force coefficient, $F_Y/q_\infty S$
C_Z	normal-force coefficient, $F_Z/q_\infty S$
$\bar{c}$	wing mean aerodynamic chord, m (ft)
F_D	drag force, N (lbf)
F_L	lift force, N (lbf)
F_X	longitudinal force, N (lbf)
F_Y	side force, N (lbf)
F_Z	normal force, N (lbf)
h	altitude, m (ft)
I_X	moment of inertia about longitudinal body axis, kg-m^2 (slug-ft^2)
I_Y	moment of inertia about lateral body axis, kg-m^2 (slug-ft^2)
I_Z	moment of inertia about normal body axis, kg-m^2 (slug-ft^2)
L/D	lift-drag ratio
M_X	rolling moment, m-N (ft-lbf)
M_Y	pitching moment, m-N (ft-lbf)
M_Z	yawing moment, m-N (ft-lbf)
m	glider mass, kg (slugs)
p	rolling velocity, rad/sec or deg/sec
q	pitching velocity, rad/sec or deg/sec
q_∞	free-stream dynamic pressure, N/m^2 (lbf/ft^2)

[redacted]

r	yawing velocity, rad/sec or deg/sec
S	wing area, m^2 (ft^2)
t	time, sec
$t_{1/2}$	time required for amplitude of oscillation to decrease by a factor of 2, sec
V	velocity, m/sec (ft/sec)
α	angle of attack, deg or rad
β	angle of sideslip, deg or rad
γ	flight-path angle, deg or rad
θ	inclination of X body axis with respect to horizon
μ	relative density parameter, $m/\rho Sb$
ρ	mass density of air or water, kg/m^3 ($slugs/ft^3$)
ϕ	angle of bank, deg or rad
ψ	angle of yaw, deg or rad

Coefficients:

$$C_{X_q} = \frac{\partial C_X}{\partial \frac{q\bar{c}}{2V}} \qquad C_{Z_q} = \frac{\partial C_Z}{\partial \frac{q\bar{c}}{2V}} \qquad C_{m_q} = \frac{\partial C_m}{\partial \frac{q\bar{c}}{2V}}$$

$$C_{l_\beta} = \frac{\partial C_l}{\partial \beta} \qquad C_{n_\beta} = \frac{\partial C_n}{\partial \beta} \qquad C_{Y_\beta} = \frac{\partial C_Y}{\partial \beta}$$

$$C_{l_p} = \frac{\partial C_l}{\partial \frac{pb}{2V}} \qquad C_{n_p} = \frac{\partial C_n}{\partial \frac{pb}{2V}} \qquad C_{Y_p} = \frac{\partial C_Y}{\partial \frac{pb}{2V}}$$

$$C_{l_r} = \frac{\partial C_l}{\partial \frac{rb}{2V}} \qquad C_{n_r} = \frac{\partial C_n}{\partial \frac{rb}{2V}} \qquad C_{Y_r} = \frac{\partial C_Y}{\partial \frac{rb}{2V}}$$

[redacted]

DESCRIPTION OF GLIDER

A three-view sketch showing the general layout of the glider configuration is presented in figure 1 and the mass and geometric characteristics of the vehicle are given in table I. The configuration utilized deployable (spring-loaded) aluminum sheet metal wings, a hardwood fuselage, and sheet metal tail surfaces. As indicated in table I, the nominal glider mass of 0.68 kg (0.0466 slug) resulted in a high value of the relative density μ (approximately 93.3 for the vehicle in air at 609.6 m (2000 ft)).

One of the most important geometric features of the glider was the wing construction and shape. The wing panels were stamped aluminum slabs shaped to a 10-percent mean camber line. The techniques involved in the construction of the wings and mating of the wing panels to the fuselage were not under precise quality control, and it will subsequently be shown that aerodynamic characteristics arising from model asymmetries were an important factor in the unsuccessful flight tests.

METHOD OF ANALYSIS

Static wind-tunnel force tests were conducted to determine the longitudinal and lateral directional aerodynamic characteristics of the glider for the two vertical-tail configurations shown in figure 1. Dynamic stability derivatives of the glider were estimated by use of the methods of reference 1. The static and dynamic aerodynamic stability derivatives were used as input data for theoretical calculations of the lateral-directional dynamic stability characteristics using linear three-degrees-of-freedom equations of motion. In addition, time histories of flight motions were generated by use of a nonlinear six-degrees-of-freedom digital computer program.

Wind Tunnel

The static aerodynamic data presented herein were obtained at the Langley Research Center with a representative glider in a low-speed wind tunnel with a 3.66-m (12-ft) octagonal test section. The model was strut mounted to a small six-component strain-gage balance. Tests were conducted with the glider erect and inverted in order to determine longitudinal flow angularity, and a flow survey was made to determine the directional flow angularity. The test apparatus was alined with the flow so that the glider was at $\beta = 0^{\circ}$ for $\alpha = 0^{\circ}$.

Tests

Static force tests were conducted in the low-speed wind tunnel at a Reynolds number of approximately 0.04×10^6 based on the mean aerodynamic chord of the wing. During the

tests, measurements were made of the six force and moment components for a center-of-gravity location corresponding to $0.25\bar{c}$ over an angle-of-attack range of -10° to 20° for a range of angles of sideslip of $\pm 10^{\circ}$.

Calculations

The dynamic stability characteristics of the lateral-directional modes of motion were calculated for the glider with each of the vertical tails shown in figure 1 by using the linearized three-degrees-of-freedom equations of motion presented in reference 2. The calculated characteristics included the time to half-amplitude $t_{1/2}$ of the Dutch roll mode, spiral mode, and roll-subsidence modes.

Motions of the glider in air and in water were calculated by using a nonlinear, six-degrees-of-freedom computer program. Use of the nonlinear program was necessitated by the large, rapid angular motions exhibited by the glider in air.

RESULTS OF FORCE TESTS

Longitudinal Characteristics

The static longitudinal aerodynamic characteristics of the configuration are presented in figure 2 for the complete configuration and the configuration with the horizontal tails removed. The data show that the basic configuration exhibited good longitudinal stability (negative, linear variation of C_m with α) and that the horizontal tail provided a contribution to longitudinal stability which was essentially constant over the angle-of-attack range of the tests. The data also indicate that the glider would trim at an angle of attack of about 2° with a value of L/D of about 5.2. During the longitudinal-force tests, a limited number of tuft flow-visualization tests were conducted to determine the flow conditions over the wing panels. The results of these flow-visualization tests indicated that the onset of wing stall occurred near $\alpha = 2^{\circ}$; this result is in agreement with the static longitudinal data presented in figure 2. The flow-visualization tests also indicated that the wings were completely stalled at $\alpha = 5^{\circ}$. Thus, the proximity of the trim angle of attack to the stall may have been the factor which resulted in the sudden wing drop following an initial pullout from launch.

Lateral-Directional Characteristics

Some of the more important lateral-directional aerodynamic characteristics of the glider are presented in figure 3 for the configuration with the small and large vertical tails and for the configuration with the vertical tail removed. The data are presented in terms of the static directional stability derivative C_{n_β} and the effective dihedral derivative C_{l_β}, obtained over a range of sideslip angle of $\pm 5^{\circ}$. Figure 3 also presents the variation of rolling-moment coefficient at zero sideslip $C_{l,0}$ with angle of attack.

The variations of C_{n_β} and C_{l_β} with α show that the configuration exhibited positive directional stability (positive values of C_{n_β}) and positive effective dihedral (negative values of C_{l_β}) over the range of angle of attack with either vertical tail.

The factor most nearly relating to observed flight behavior difficulties was the indication that significant out-of-trim rolling moments existed for the configuration within the intended operational range of angle of attack. As shown in figure 3, the magnitude of the rolling-moment coefficient at $\beta = 0^\circ$ was large over the region of interest. For purposes of comparison, the magnitude of the rolling-moment coefficient measured at $\alpha = 0^\circ$ was about equal to the magnitude obtained for full aileron deflection on conventional airplanes. The large out-of-trim values of $C_{l,0}$ were probably caused by difficulties associated with holding close tolerances by use of simple manufacturing techniques.

RESULTS OF CALCULATIONS

Dynamic Stability Characteristics

The results of calculations to determine the lateral-directional dynamic stability characteristics of the configuration for the two vertical-tail sizes used by the contractor are presented in figure 4. The experimentally determined values of the static derivatives, and the estimated values of the dynamic derivatives (see ref. 1) used in the calculations of the dynamic stability characteristics herein, are presented in table II.

The results of the calculations for trimmed flight at various angles of attack for an altitude of 609.6 m (2000 ft) are presented in figure 4 in terms of the damping factor $1/t_{1/2}$ of the roll, spiral, and Dutch roll modes. Positive values of $1/t_{1/2}$ represent damped (dynamically stable) modes whereas negative values represent undamped (dynamically unstable) modes. The results of these calculations show that with the large vertical tail (fig. 4(a)), the configuration would be expected to exhibit an unstable spiral mode throughout the angle-of-attack range considered, and that the stability of all the modes decreased with increasing angle of attack. With the small vertical tail (fig. 4(b)), the results indicate the existence of an unstable Dutch roll mode for angles of attack from 0° to 6°. An additional factor relating to the unsuccessful free-flight tests therefore appears to be the inherent dynamic instability of the configuration.

Presented in figure 5 are boundaries for spiral stability and oscillatory (Dutch roll) stability in terms of variations of the stability derivatives C_{n_β} and C_{l_β} for the configuration at $\alpha = 2^\circ$. Values of C_{n_β} and C_{l_β} are also indicated for the glider with the small and large vertical tails. The locations of these values relative to the spiral and oscillatory boundaries further illustrate the inherent dynamic stability problem, and the data also indicate that a stable region can be obtained with suitable values of C_{n_β} and C_{l_β}.

The data of figure 5 also indicate that the dynamic stability characteristics exhibited by the configuration may be vastly different in water. Although the spiral stability boundary is independent of the relative density of the glider, the dashed line in figure 5 shows that the oscillatory stability boundary becomes markedly less restrictive, with the result that there is a much larger region of stability. It would appear, therefore, that the glider configuration would exhibit unrealistically good oscillatory stability in the swimming pool tests.

Calculated Flight Motions

Presented in figures 6, 7, and 8 are calculated time histories of flight motions for the glider in air and in water. The initial conditions for the calculations are as follows:

Condition	Initial condition in –	
	Air	Water
h, m (ft)	609.6 (2000)	1.83 (6)
V, m/sec (ft/sec)	30.48 (100)	0.91 (3)
α, deg	3	3
β, deg	1	1
ρ, kg/m^3 (slugs/ft^3)	1.154 (0.00224)	999.66 (1.94)
ψ, deg	0	0
θ, deg	-3	-3
ϕ, deg	0	0

Shown in figure 6(a) are the calculated motions for the configuration with the large vertical tail. The Dutch roll oscillation is seen to be stable (as expected based on the data of fig. 4) as evidenced by the variations in the heading ψ. After the initial disturbance, the motions damp out and the glider trims at $\alpha = 2^{\circ}$. As time progresses, the spiral instability previously discussed for this configuration begins to appear in the form of continuously increasing values of bank angle ϕ and heading ψ. The total flight time from launch at h = 609.6 m (2000 ft) to impact at h = 0 is approximately 142 seconds.

The time history for the glider with the small vertical tail is presented in figure 6(b). The motion is characterized initially by the extremely unstable Dutch roll oscillation, previously discussed for this configuration, which is seen to build up to a limit cycle oscillation for which variations in bank angles of $\pm 80^{\circ}$ occurred. This condition resulted in a significant decrease in total flight time to approximately 78 seconds (as compared with 142 seconds for the configuration with the larger vertical tail).

Although the foregoing calculated motions may appear to be acceptable for the glider, it must be remembered that the effects of asymmetric wing stall have not been simulated. Additionally, these results have been obtained by use of relatively small disturbances from the trim condition, whereas larger disturbances would be expected to yield significantly larger amplitude motions which may result in completely unacceptable behavior.

Figure 7 presents the results of time history calculations to determine the effects of out-of-trim rolling moments. The calculations were made for the configuration with both the large and small vertical tails and included the values of out-of-trim rolling moment shown in figure 3. The results of the calculations show that for both tail sizes considered, the configuration immediately developed a large roll rate which resulted in a continuous 360° rolling motion. As a result of the rolling motion, the glider followed an essentially ballistic trajectory and reached $h = 0$ at $t = 14.5$ sec. This result is in good agreement with flight-test results and appears to indicate that the primary factor causing the rapid rolling motion was the out-of-trim rolling moment.

Since the models with the small vertical tail were observed to exhibit satisfactory behavior when tested in water, additional time histories were computed to simulate this condition. The time histories in figure 8(a) show the motion of the glider in water for the case of no rolling-moment asymmetry. The configuration exhibits excellent flight characteristics with a heavily damped Dutch roll oscillation, as expected, based on the data of figure 5 which show the marked shift in the oscillatory stability boundary when the density increases from that of air to that of water. Figure 8(b) shows the time histories for the configuration in water with the out-of-trim rolling moments included. The configuration developed a relatively small roll rate and exhibited steady turning flight with a bank angle of approximately 1°.

The differences between the mild turn exhibited by the configuration in water and the ballistic flight path determined in air can be explained by consideration of the relationship between the rolling-moment coefficient required for steady turning flight $C_{l,0}$ and the relative density parameter μ. An approximate expression showing this relationship is developed in the appendix as

$$C_{l,0} \approx \frac{\left[C_L \cos(-\gamma) + C_D \sin(-\gamma)\right]\left[\left(C_{l_\beta}C_{n_r} - C_{n_\beta}C_{l_r}\right)\cos\phi + \left(C_{n_\beta}C_{l_p} - C_{l_\beta}C_{n_p}\right)\theta\right]\sin\phi}{4\mu C_{n_\beta}}$$

Using the measured and estimated values of the stability derivatives at the trim condition thus defines this relationship which is plotted in figure 9 with a parametric dependence on the bank angle ϕ. From figure 9 it is seen that for the level of asymmetry considered herein, the vehicle would be expected to turn with a bank angle of approximately 1°

in water. This result correlates with the time history calculations shown in figure 8(b). Additionally, from figure 9 the vastly larger relative density of the vehicle in air places the configuration in a region for which no steady-state equilibrium turn is possible. Thus, in air, the out-of-trim rolling moment would be expected to cause the vehicle to develop a large body axis roll rate, which would then result in an essentially ballistic trajectory. This result correlates with the time history calculations shown in figure 7, and with the experimental flight-test results.

SUMMARY OF RESULTS

The results of an investigation to determine the stability characteristics of a deployable small glider, with folding wings, have indicated the following possible causes for a series of unsuccessful test flights:

1. The proximity of the trim condition to the onset of wing stall
2. The inherent lateral-directional instability of the configuration
3. The existence of large out-of-trim rolling moments created by wing asymmetries.

Langley Research Center,
National Aeronautics and Space Administration,
Hampton, Va., January 28, 1975.

[redacted]

APPENDIX

ROLLING MOMENT REQUIRED FOR STEADY TURNING FLIGHT

An approximate expression for the rolling-moment coefficient required for steady turning flight $C_{l,0}$ as a function of the relative density parameter μ is developed through consideration of the forces and moments acting on the vehicle shown in figure 10 where R is the radius of turn, γ is the flight-path angle, and Ω is the turn rate. Centripetal equilibrium requires

$$\left[F_L \cos(-\gamma) + F_D \sin(-\gamma)\right] \sin\phi + F_Y \cos\phi = \frac{mV^2}{R} \tag{A1}$$

Nondimensionalizing equation (A1) and neglecting the side force yields

$$\left[C_L \cos(-\gamma) + C_D \sin(-\gamma)\right] \sin\phi \approx \frac{2m}{R\rho S} \tag{A2}$$

An approximate form of the yawing- and rolling-moment equations may be written as follows:

$$C_{n_\beta}\beta + C_{n_p}\frac{pb}{2V} + C_{n_r}\frac{rb}{2V} \approx 0 \tag{A3}$$

$$C_{l_\beta}\beta + C_{l_p}\frac{pb}{2V} + C_{l_r}\frac{rb}{2V} + C_{l,0} \approx 0 \tag{A4}$$

If small values of θ are assumed, the following approximate expressions for the nondimensional rolling and yawing velocities result:

$$\frac{pb}{2V} \approx -\frac{\Omega b}{2V}\theta \tag{A5}$$

$$\frac{rb}{2V} \approx \frac{\Omega b}{2V}\cos\phi \tag{A6}$$

The assumption of small values of γ yields

$$\frac{\Omega b}{2V} \approx \frac{b}{2R} \tag{A7}$$

Substituting equation (A7) into equation (A2) and equations (A5) and (A6) into equations (A3) and (A4) yields the following set of approximate expressions:

$$\left[C_L \cos(-\gamma) + C_D \sin(-\gamma)\right] \sin\phi \approx 4\mu\frac{\Omega b}{2V} \tag{A8}$$

$$C_{n_\beta}\beta + \left(C_{n_r} \cos \phi - C_{n_p}\theta\right)\frac{\Omega b}{2V} \approx 0 \tag{A9}$$

$$C_{l_\beta}\beta + \left(C_{l_r} \cos \phi - C_{l_p}\theta\right)\frac{\Omega b}{2V} + C_{l,0} \approx 0 \tag{A10}$$

Solving equations (A9) and (A10) for $\Omega b/2V$ and substituting this result into equation (A8) yields upon rearranging

$$C_{l,0} = \frac{\left[C_L \cos(-\gamma) + C_D \sin(-\gamma)\right]\left[\left(C_{l_\beta}C_{n_r} - C_{n_\beta}C_{l_r}\right) \cos \phi + \left(C_{n_\beta}C_{l_p} - C_{l_\beta}C_{n_p}\right)\theta\right] \sin \phi}{4\mu C_{n_\beta}} \tag{A11}$$

Equation (A11) is an approximate expression for the rolling-moment coefficient required for steady turning flight $C_{l,0}$ as a function of the relative density parameter μ and the bank angle ϕ.

REFERENCES

1. Campbell, John P.; and McKinney, Marion O.: Summary of Methods for Calculating Dynamic Lateral Stability and Response and for Estimating Lateral Stability Derivatives. NACA Rep. 1098, 1952. (Supersedes NACA TN 2409.)

2. Chambers, Joseph R.; and Anglin, Ernie L.: Analysis of Lateral-Directional Stability Characteristics of a Twin-Jet Fighter Airplane at High Angles of Attack. NASA TN D-5361, 1969.

[redacted]

TABLE I.- MASS AND GEOMETRIC CHARACTERISTICS OF THE GLIDER

Mass (nominal), kg (slugs)	0.68 (0.0466)
Moments of inertia, kg-m^2 (slug-ft^2):	
I_X	0.0020 (0.0015)
I_Y	0.0027 (0.0020)
I_Z	0.0045 (0.0033)
Overall length, cm (in.)	26.16 (10.3)
Wing:	
Span, cm (in.)	40.64 (16.0)
Area, cm^2 (in^2)	154.84 (24.0)
Mean aerodynamic chord, cm (in.)	3.81 (1.5)
Aspect ratio	10.67
Taper ratio	1.0
Dihedral, deg	3.0
Incidence, deg	3.5
Airfoil section	10-percent-camber line metal slab
Horizontal tail:	
Span, cm (in.)	15.24 (6.0)
Area, cm^2 (in^2)	58.06 (9.0)
Mean aerodynamic chord, cm (in.)	3.81 (1.5)
Aspect ratio	4.0
Taper ratio	1.0
Dihedral	0
Incidence, deg	-1.5
Airfoil section	Metal slab
Large vertical tail:	
Span, cm (in.)	6.35 (2.5)
Area, cm^2 (in^2)	26.19 (4.06)
Root chord, cm (in.)	4.70 (1.85)
Tip chord, cm (in.)	3.56 (1.4)
Airfoil section	Metal slab
Small vertical tail:	
Span, cm (in.)	3.81 (1.5)
Area, cm^2 (in^2)	16.19 (2.51)
Root chord, cm (in.)	4.70 (1.85)
Tip chord, cm (in.)	3.81 (1.5)
Airfoil section	Metal slab

TABLE II.- STABILITY DERIVATIVES

(a) Lateral

Derivative	Value for –							
	Large vertical tail at α of –				Small vertical tail at α of –			
	0^o	4^o	8^o	12^o	0^o	4^o	8^o	12^o
C_{Y_β}	-0.470	-0.470	-0.540	-0.610	-0.068	-0.068	-0.202	-0.270
C_{n_β}	.200	.200	.230	.260	.029	.029	.086	.115
C_{l_β}	-.172	-.200	-.172	-.200	-.200	-.200	-.212	-.218
C_{Y_p}	0	0	0	0	0	0	0	0
C_{n_p}	-.05	0	.06	.06	-.05	0	.06	.06
C_{l_p}	-.70	-.37	-.26	-.06	-.70	-.37	-.26	-.06
C_{Y_r}	.40	.40	.46	.52	.06	.06	.17	.23
C_{n_r}	-.28	-.29	-.33	-.36	-.14	-.14	-.20	-.23
C_{l_r}	.25	.40	.43	.47	.27	.40	.48	.49

(b) Longitudinal

$C_{X_q} = 0$ $\quad C_{Z_q} = 0$ $\quad C_{m_q} = -45.0$

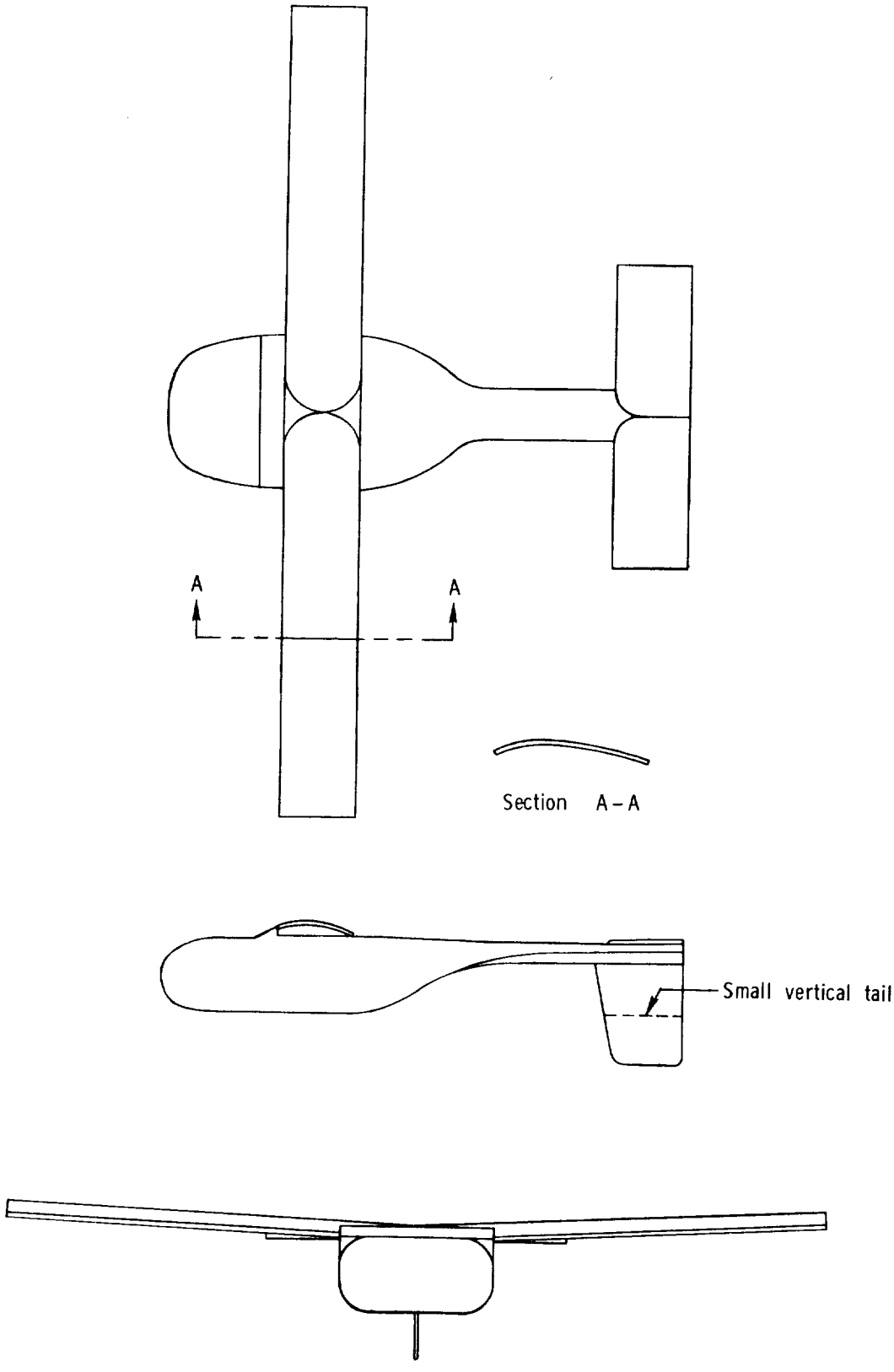

Figure 1.- Three-view sketch of glider configuration.

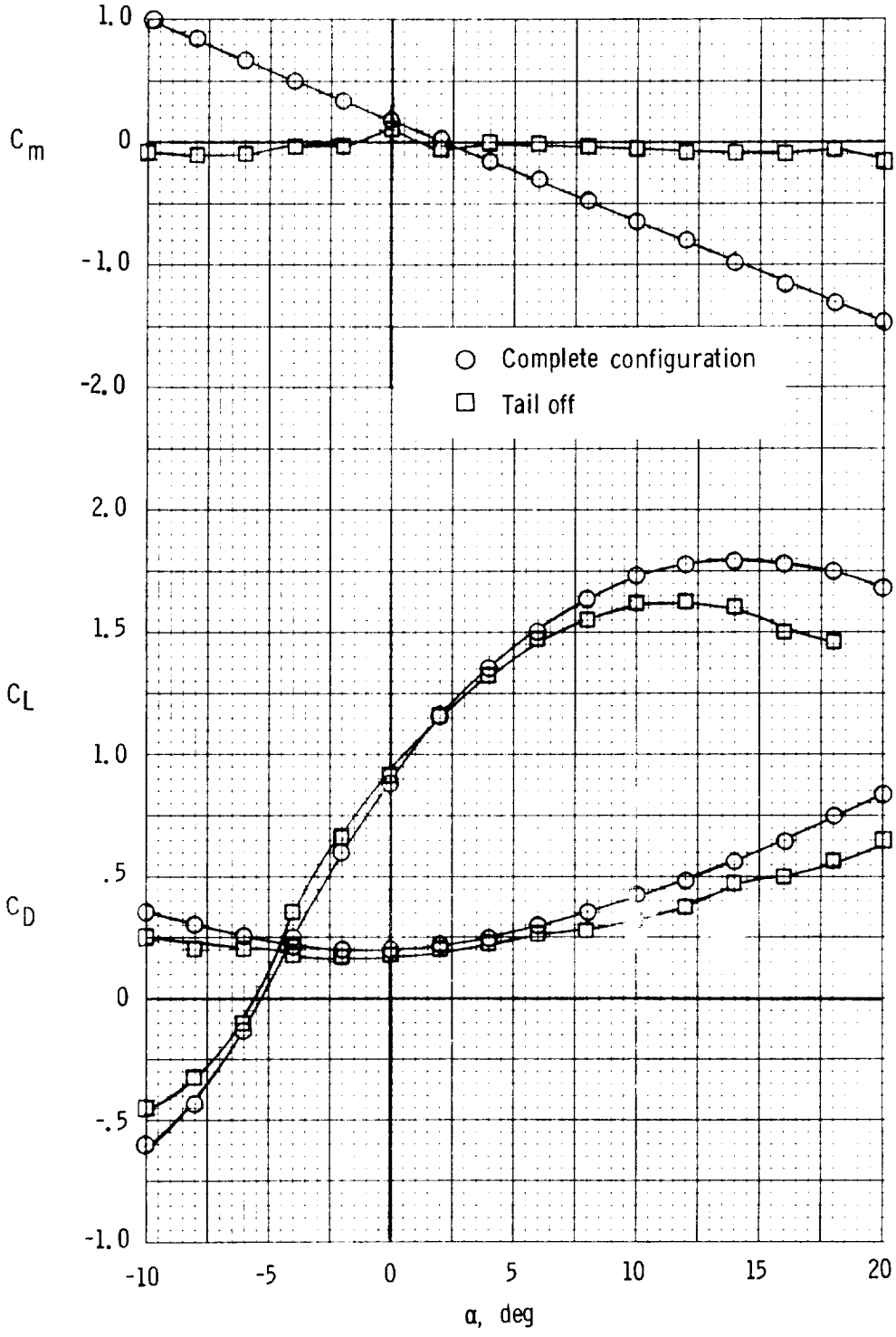

Figure 2.- Variation of static longitudinal characteristics with angle of attack.

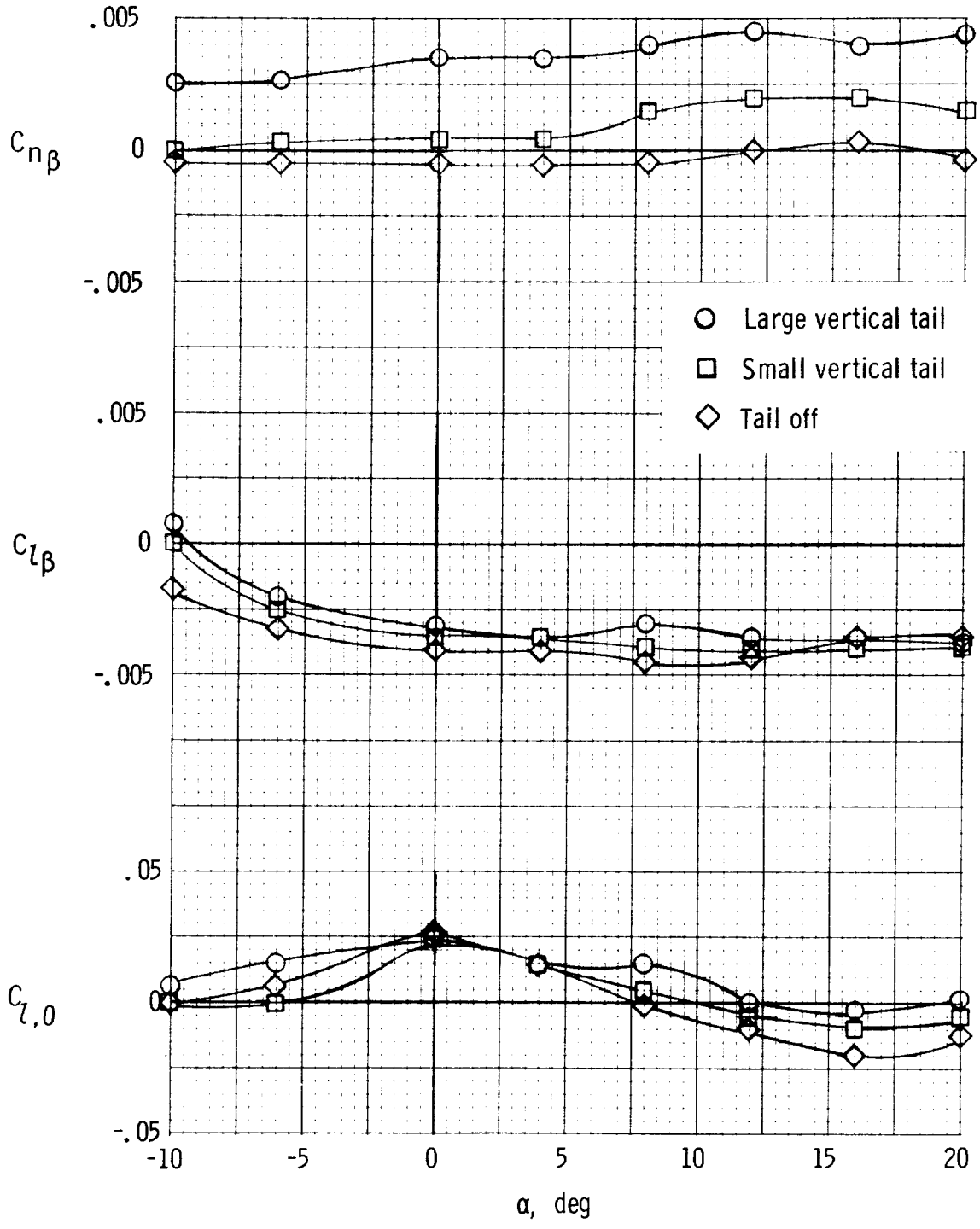

Figure 3.- Variation of static lateral characteristics with angle of attack.

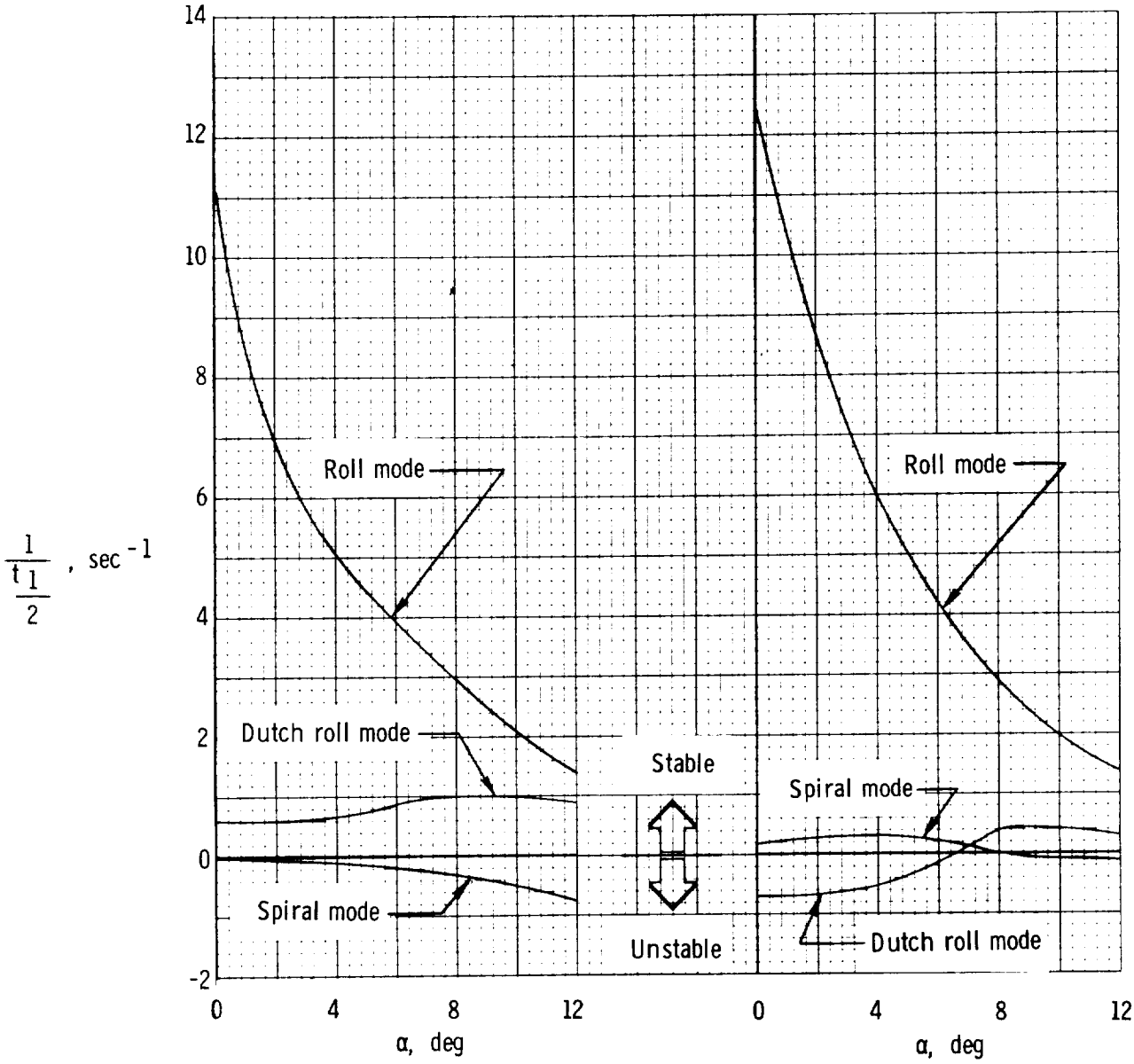

(a) Large vertical tail.

(b) Small vertical tail.

Figure 4.- Results of dynamic stability calculations.

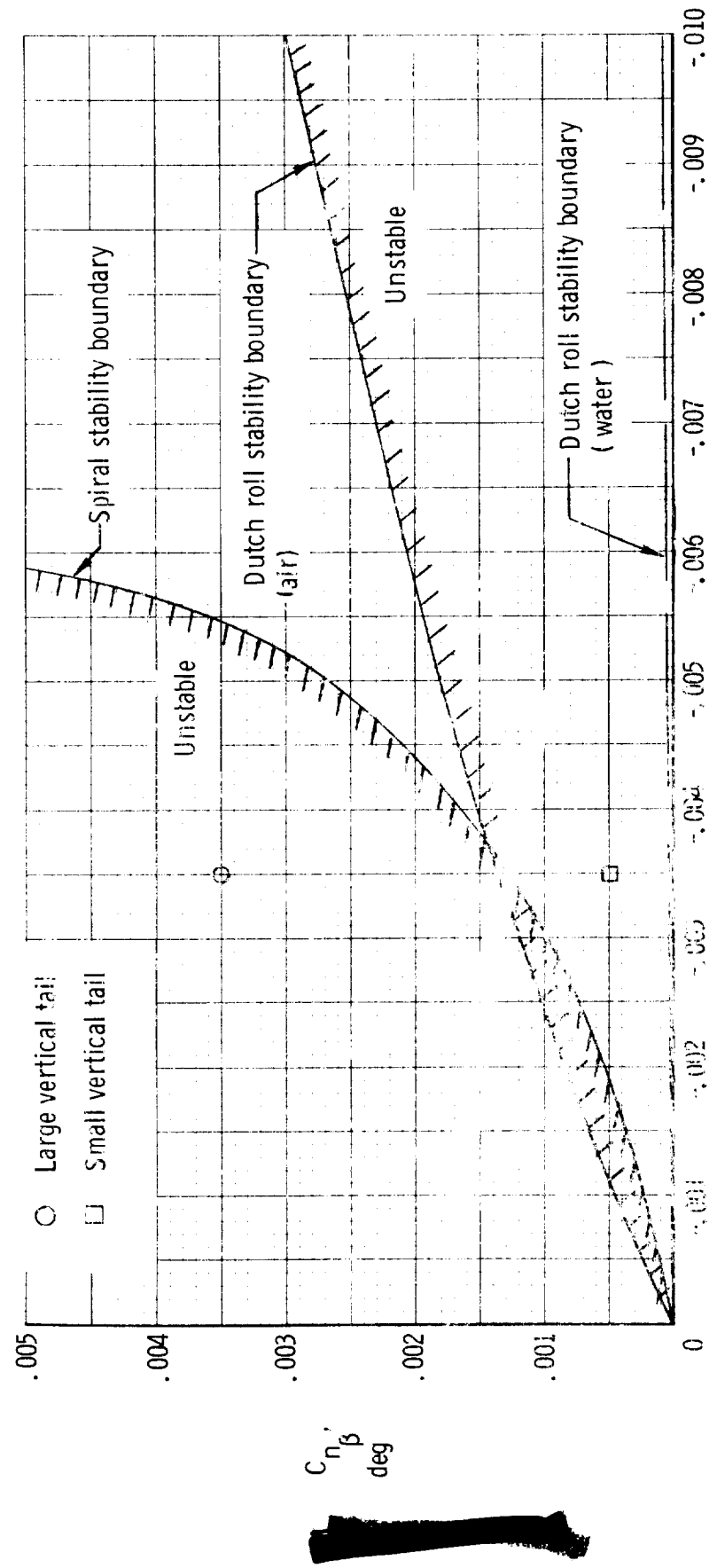

Figure 5.- Lateral stability boundaries. $\alpha = 2^{\circ}$.

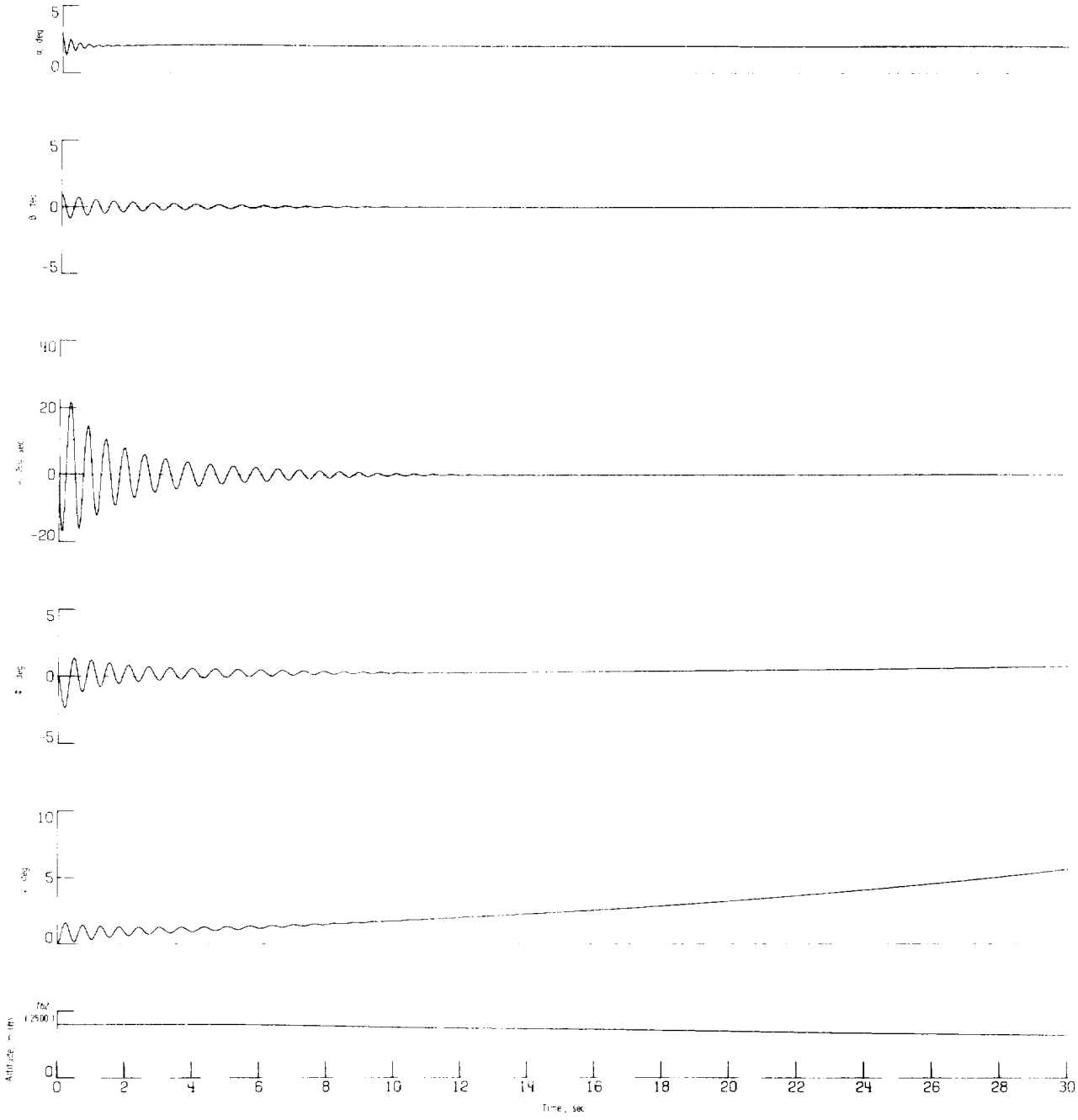

(a) Configuration with large vertical tail.

Figure 6.- Calculated time history of flight motions in air. (Out-of-trim rolling moment not included.)

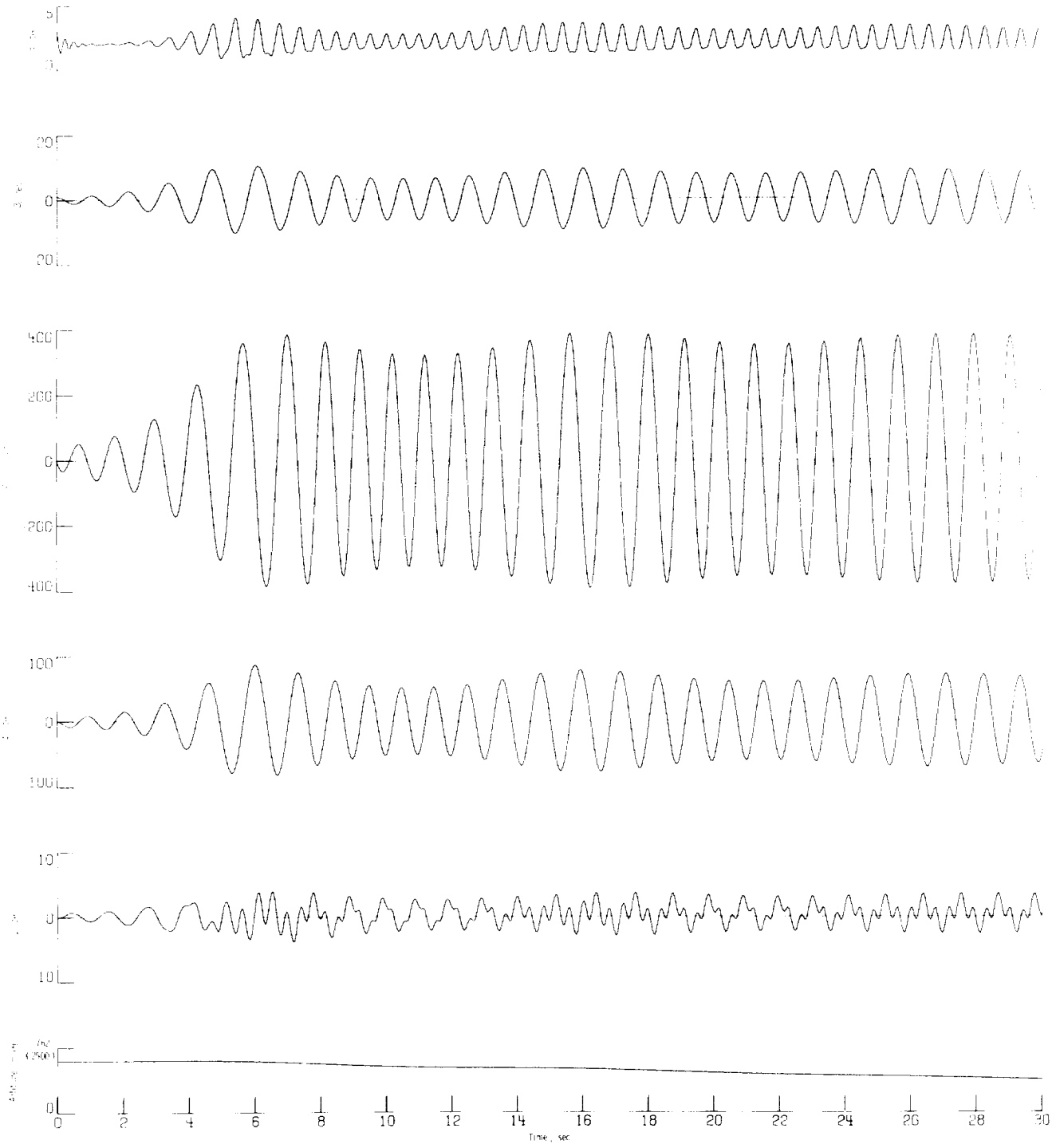

(b) Configuration with small vertical tail.

Figure 6.- Concluded.

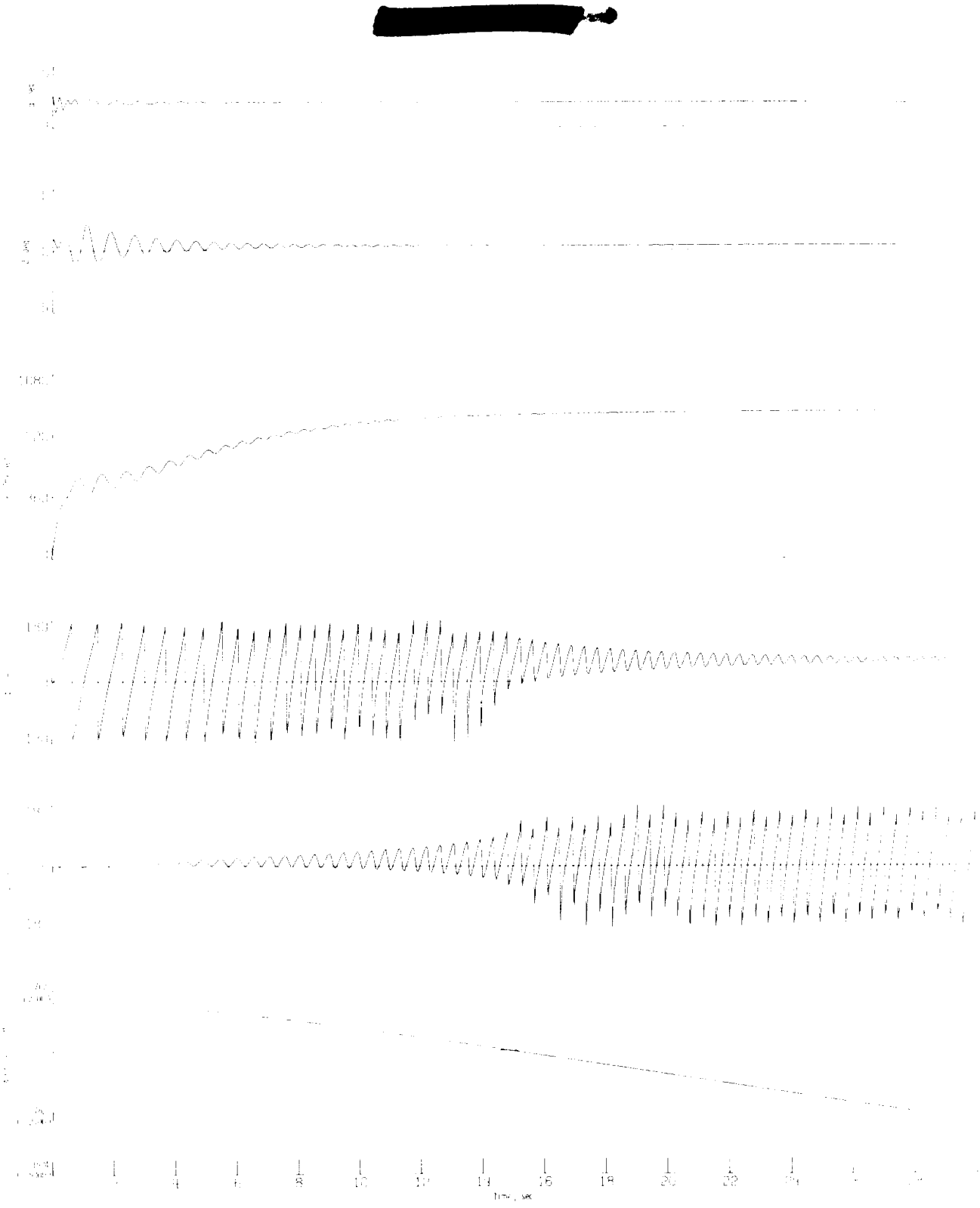

(a) Configuration with large vertical tail.

Figure 7.- Calculated time history of flight motions in air. (Out-of-trim rolling moment included.)

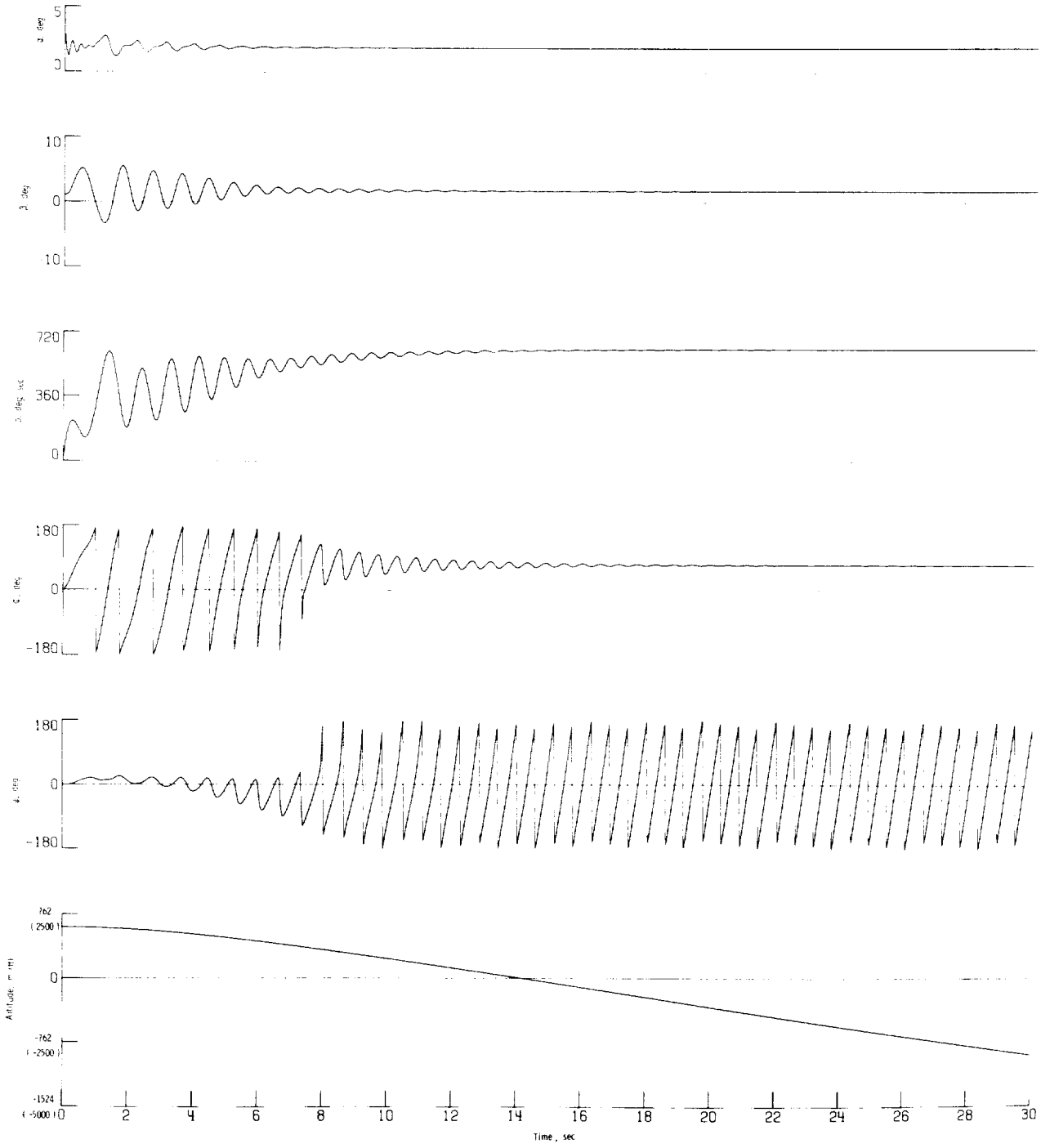

(b) Configuration with small vertical tail.

Figure 7.- Concluded.

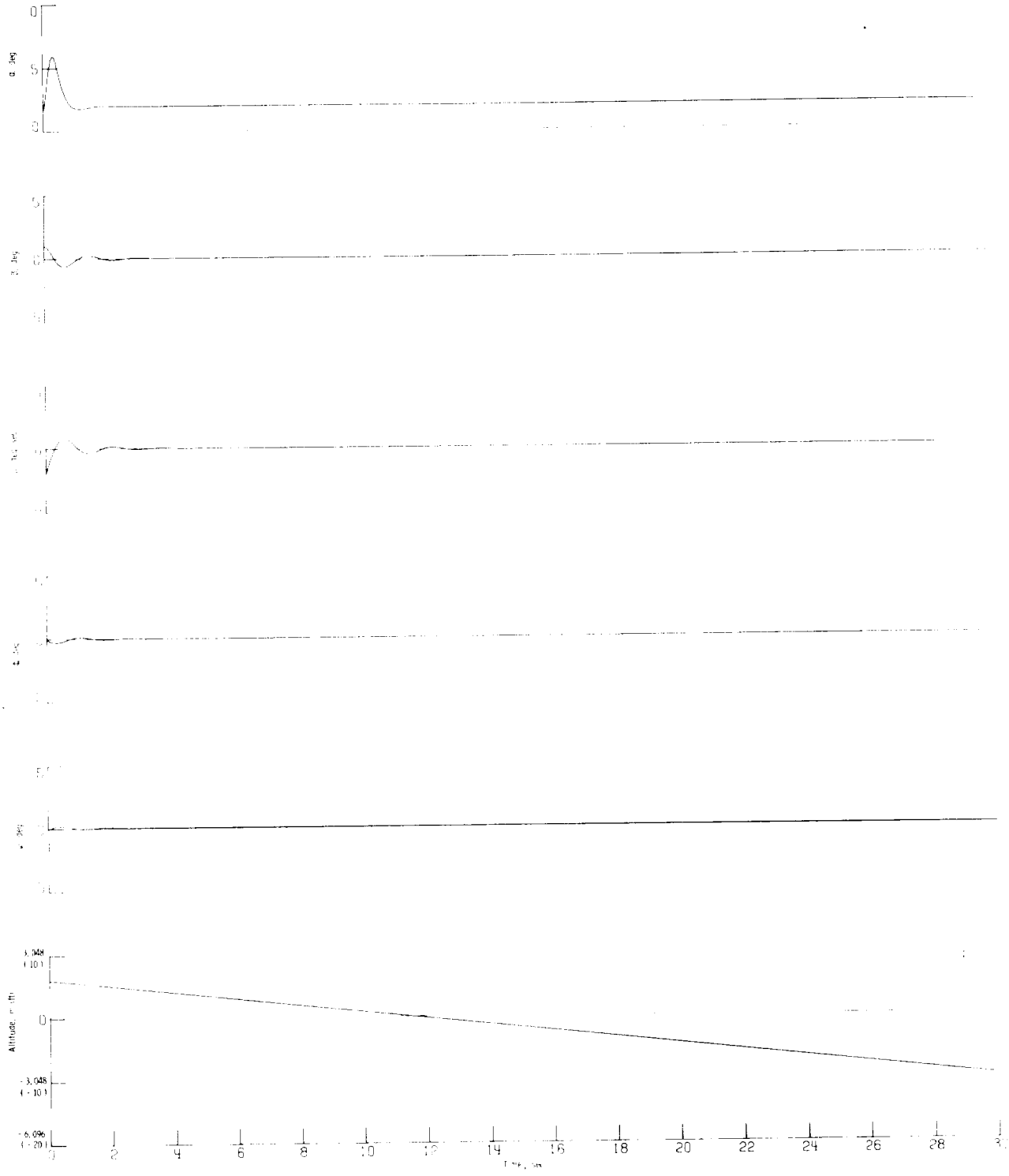

(a) Out-of-trim rolling moment not included.

Figure 8.- Calculated time history of motions in water. (Configuration with small vertical tail.)

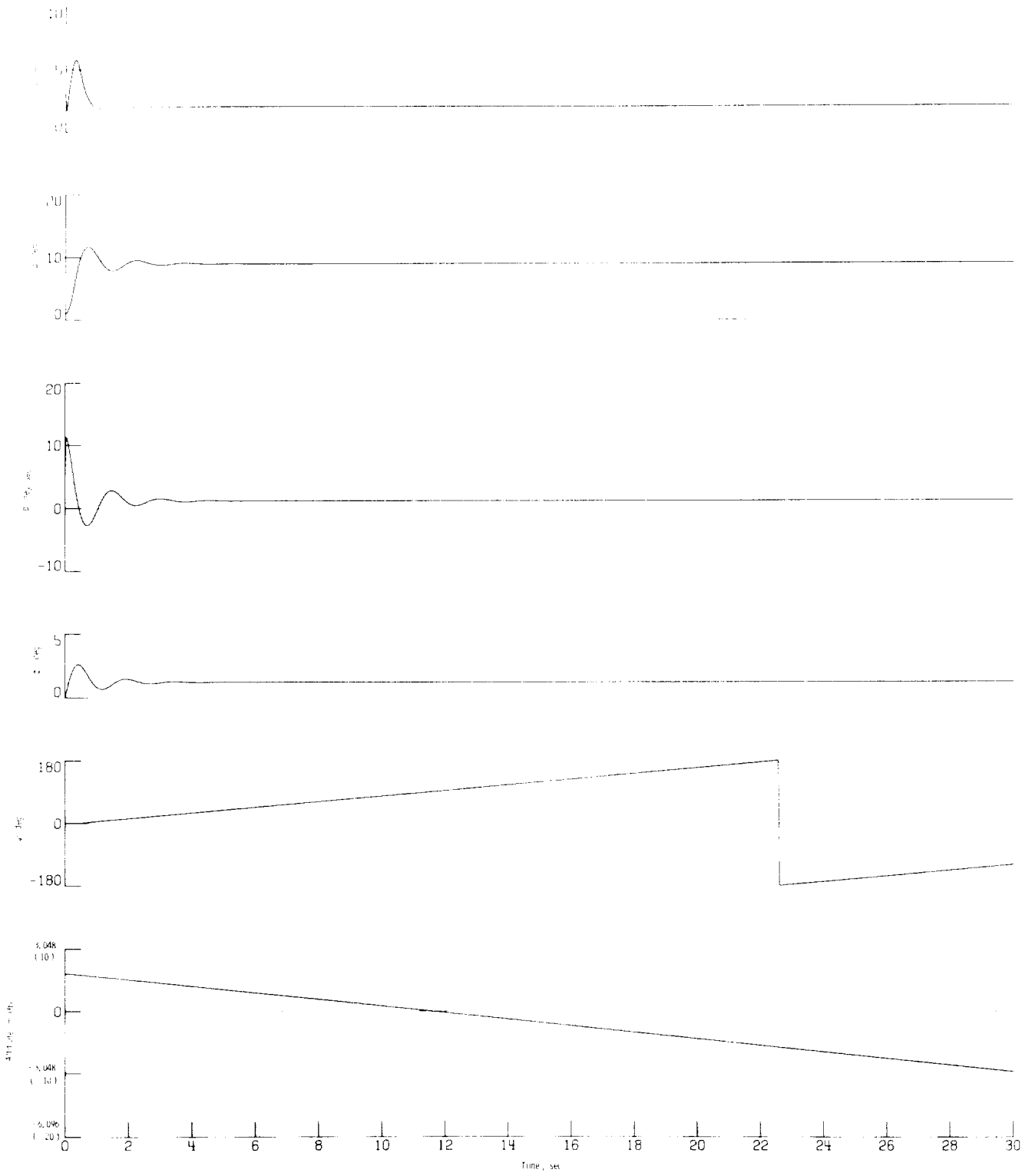

(b) Out-of-trim rolling moment included.

Figure 8.- Concluded.

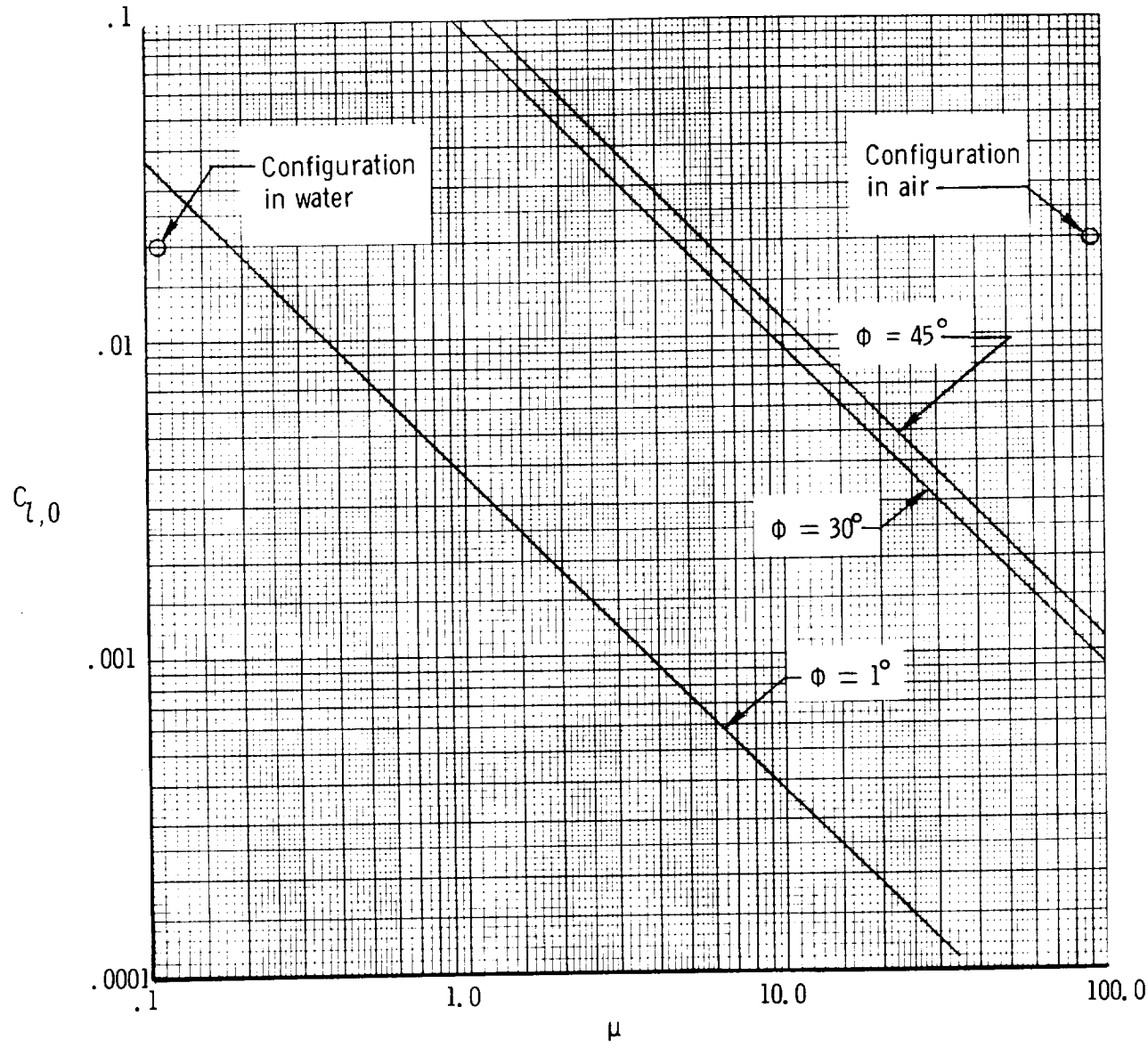

Figure 9.- Approximate variation of rolling-moment coefficient required for steady-state turn. Configuration with small vertical tail; $\alpha = 2^{\circ}$.

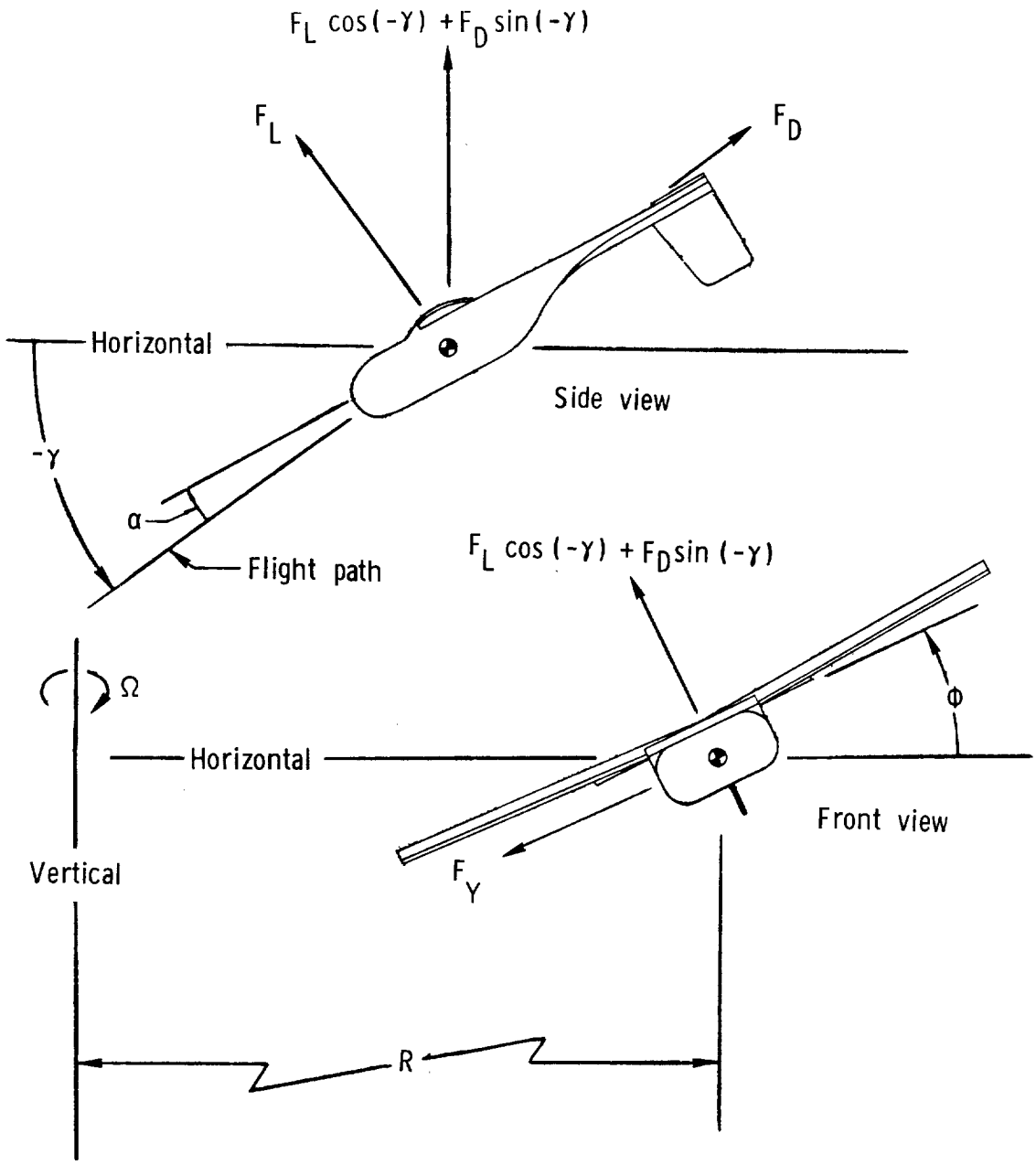

Figure 10.- Sketch of vehicle performing steady-state turn.